

# Low-Drift Coherent Population Trapping Clock Based on Laser-Cooled Atoms and High-Coherence Excitation Fields

Xiaochi Liu, Eugene Ivanov, Valeriy I. Yudin, John Kitching, and Elizabeth A. Donley\*

*National Institute of Standards and Technology, 325 Broadway, Boulder, Colorado 80305, USA*

(Received 2 August 2017; revised manuscript received 22 September 2017; published 2 November 2017)

A compact cold-atom coherent population trapping clock in which laser-cooled atoms are interrogated with highly coherent coherent population trapping fields under free fall is presented. The system achieves fractional frequency instability at the level of  $3 \times 10^{-13}$  on the time scale of an hour. The clock may lend itself to portable applications since the atoms typically fall only 1.6 mm during the typical interrogation period of 18 ms.

DOI: 10.1103/PhysRevApplied.8.054001

## I. INTRODUCTION

Compact, high-performance atomic clocks are used widely in many applications, and the market for commercial atomic clocks is heavily dominated by microwave clocks. There is continuous interest in exploring alternative interrogation techniques to either improve clock performance or expand applications by achieving smaller size, weight, and power. Most commercial microwave atomic clocks are based on direct microwave interrogation [1–3], but the interrogation of the microwave transitions can also be performed optically with coherent population trapping (*CPT*) [4–6]. Since no microwave cavity is needed, *CPT* atomic clocks have an advantage for volume and power consumption, which is a factor that enabled the development of chip-scale atomic clocks [7,8].

Vapor-cell *CPT* clocks have demonstrated outstanding short-term instabilities [9,10], but their frequency instability on time scales longer than a few-hundred seconds has been limited by drifts that correlate with changes in temperature, laser power, and laser frequency [9–12]. Fundamentally, these drifts arise from buffer-gas shifts and light shifts.

The buffer gases that are used to extend the period between wall collisions [13] introduce pressure- and temperature-dependent shifts that can be large. The temperature coefficient for the change in fractional frequency of high-performance buffer-gas *CPT* clocks has been measured to be of order  $10^{-10}/\text{K}$  [14–16] or slightly better [9], requiring millikelvin-level temperature stability to stabilize the fractional frequency at the  $10^{-13}$  level.

Light shifts can also degrade the long-term stability of *CPT* clocks [9,10,17]. These shifts arise from both resonant interactions when incomplete dark states are formed [18,19] and traditional ac-Stark shifts from off-resonant interactions [17]. These light shifts cause frequency shifts that depend on laser power and laser frequency, as well as on the power of the microwave signal that is used for the

phase modulation to produce the *CPT* interrogation light [9,14,17]. Contributions from these various effects can be difficult to distinguish in vapor-cell clocks in which the optical resonances are broadened and relaxation is present.

Noise on the relative phase between the optical fields that interrogate the *CPT*  $\Lambda$  system can generate short- as well as long-term instabilities [20,21]. Such relative phase noise can be large when the optical fields are generated by phase-locked lasers, which limited previous experiments to a short-term frequency instability of  $4 \times 10^{-11}/\sqrt{\tau}$  [20]. The laser phase noise also limits the long-term stability by causing a residual resonant light shift that is proportional to optical detuning that does not vanish at high optical intensity as predicted theoretically [18,19]. The residual light shift can be explained by incomplete dark-state formation resulting from incoherent light in the *CPT* interrogation spectrum [21].

Ramsey spectroscopy [22] has been used to study *CPT* resonances in many prior studies [10,16,19,23–32]. Resonant light shifts have been shown theoretically [18,19] to scale inversely with the Ramsey period, in agreement with recent cold-atom *CPT* experiments [21]. Light shifts have also been studied using Ramsey spectroscopy in vapor-cell *CPT* clocks [10,16,32]. There, too, the shifts scale inversely with the Ramsey period. However, so far, the use of Ramsey spectroscopy has not demonstrated an improvement in long-term clock stability over continuous interrogation [10], possibly because the optimal conditions for continuous interrogation occur at a much lower intensity or because the long-term stability is limited by other effects.

To demonstrate a clock that is both compact and less sensitive to environmental perturbations, a cold-atom clock based on *CPT* and Ramsey spectroscopy has been developed [20,21]. We show here that the higher laser phase coherence achieved by the use of an electro-optic phase modulator (EOM) instead of an optical phase-lock loop (OPLL) leads to a significant improvement in the clock stability. The high-coherence light source demonstrates a resonant light shift that is at least 2 orders of magnitude

\*elizabeth.donley@nist.gov

smaller than observed in earlier experiments based on an OPLL [21] and is consistent with having no dependence on optical detuning at high intensity. Section II describes the experimental setup. Section III reports on experimental measurements that quantify the improvement in contrast, the reduction in resonant light shifts, and the improvement in frequency stability resulting from the better phase coherence of the *CPT* light. The paper concludes in Sec. IV with a discussion and summary of the experimental results that also puts this work in the context of other high-performance compact atomic clocks.

## II. EXPERIMENT

Most of the experiments have been performed with the lin || lin *CPT* scheme [33–36], for which the directions of linear polarization of the two *CPT* frequency components are parallel and orthogonal to an applied magnetic field. This configuration eliminates trap states and increases the signal-to-noise ratio (SNR) of the *CPT* resonance. In the lin || lin configuration (Fig. 1(a)), the linearly polarized and 6.835-GHz frequency-separated bichromatic light couples  $^{87}\text{Rb}$  atoms to a double- $\Lambda$  system connecting the  $|F = 1, m_F = \pm 1\rangle$  and  $|F = 2, m_F = \mp 1\rangle$  ground states via the  $|F' = 1, m_{F'} = 0\rangle$  level.

A schematic diagram of the experimental apparatus is shown in Fig. 2. The highly coherent *CPT* light is generated by a single laser using a fiber-coupled EOM. The EOM adds extra modulation sidebands to the light that do not contribute to the *CPT* signal, but since these extra sidebands are far detuned from any resonances, they do not add significantly to the light shift.

The  $^{87}\text{Rb}$  atoms are trapped in a three-dimensional magneto-optical trap (MOT) with, typically, a 25-ms cooling period and 3.5 mW of total cooling light distributed

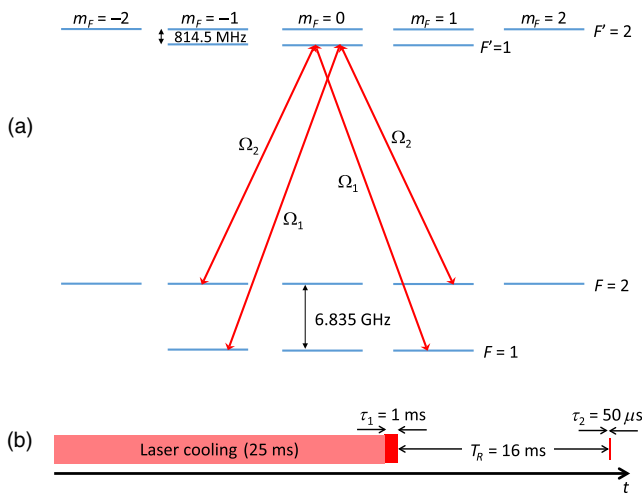


FIG. 1. (a) Energy levels in the lin || lin interrogation scheme for  $^{87}\text{Rb}$ . The Rabi frequencies of the bichromatic *CPT* light fields are  $\Omega_1$  and  $\Omega_2$ , respectively. (b) Typical timing diagram for a single shot.

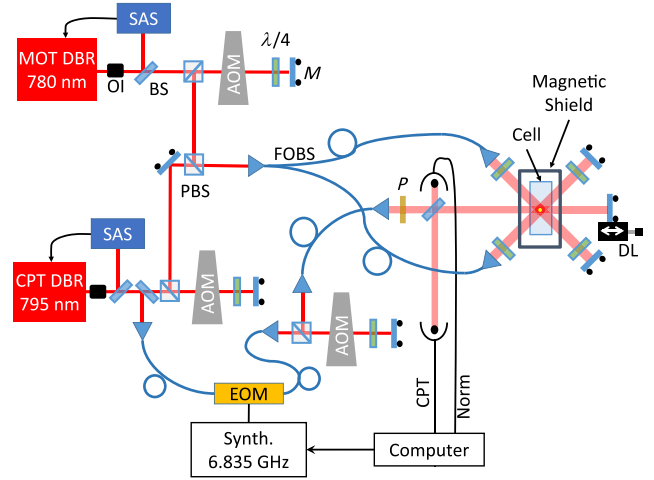


FIG. 2. Experimental apparatus. The MOT and *CPT* lasers are each offset locked from the atomic resonances with a saturated absorption spectrometer (SAS) after passing through optical isolators (OIs). There are three double-pass AOMs that shift the light to resonance and also serve as optical switches to control the on and off cycles of the laser beams. The frequency stabilized light from the *CPT* laser is used for *CPT* interrogation and also to serve as a repump for laser cooling. The repump beam is overlapped with the MOT light on a polarizing beam splitter (PBS) and injected into a 1:3 fiber-optic beam splitter (FOBS). The *CPT* beam travels horizontally through the cold atoms and is retro-reflected from a mirror attached to a translation stage that serves as a delay line (DL). The *CPT* signal is computed from the ratio of signals from the *CPT* and normalization photodiodes.

between three 7-mm-diameter input beams. The cooling light is supplied by a 780-nm distributed Bragg reflector (DBR) laser detuned by  $-12$  MHz from the  $D2$  cycling transition. There is a 2-ms optical-molasses period that follows the MOT sequence. The atoms are interrogated while under free fall after extinguishing the MOT magnetic fields and the laser-cooling beams. Because the interrogation period for Ramsey spectroscopy is typically short ( $\leq 16$  ms), most of the atoms are recaptured from cycle to cycle [37], with a typical total cycle period of 45 ms. The MOT can trap  $5 \times 10^6$  atoms in steady state. A static magnetic field of  $4.5 \mu\text{T}$  is aligned with the *CPT* laser-beam direction to lift the Zeeman degeneracy. The MOT cell is isolated from external electromagnetic perturbations with a 10-cm-diameter single-layer magnetic shield.

The *CPT* laser source is a 600-kHz-linewidth DBR laser tuned to the  $^{87}\text{Rb}$   $D1$  transitions at 795 nm. The laser is frequency stabilized by saturated absorption 170 MHz to the red of the  $F = 1$  to  $F' = 1$  optical transition. The beam is sent through a fiber-coupled EOM that is modulated at 6.835 GHz. The steering of this modulation frequency forms the digital servo that locks the atomic clock. The negative first-order sideband forms the  $\Lambda$  systems with the carrier. The output of the EOM is sent through a double-pass acousto-optic modulator (AOM), which shifts the optical frequencies to resonance, serves as an optical

switch, and is also used to control the light intensity with a feedback loop. The powers of the first-order sidebands generated by the EOM are typically set equal to the carrier signal. The total laser power incident on the atoms in the *CPT* beam varies between 2 and 30  $\mu\text{W}$ .

The modulated and switched light is coupled into a polarization-maintaining fiber, and the *CPT* beam passes through a linear polarizer to ensure the light's linear polarization is stable after the optical fiber. Then the 3.5-mm-diameter ( $1/e^2$ ) *CPT* beam is divided into two sub-beams by a 90:10 nonpolarizing beam splitter. Most of the light is sent to the normalization photodiode to stabilize the optical intensity and to use as a normalization signal to reduce the effect of intensity noise on the *CPT* signals. The weaker beam propagates through the vacuum chamber to interrogate the cold atoms. The interrogation light is reflected back by a mirror to pass through the chamber a second time and is then collected on the *CPT* photodetector. The spacing between the retroreflecting mirror and the atoms affects the *CPT* signal amplitude on length scales of half of the microwave wavelength (22 mm for  $^{87}\text{Rb}$ ) due to interference of the *CPT* coherences generated in the atoms by forward- and backward-propagating *CPT* light [38,39]. To optimize its position and maximize the *CPT* signal, the retroreflecting mirror is fixed on a translation stage to form an optical delay line, which is adjusted to achieve maximum signal amplitude and mitigate the Doppler shift [20].

The light is pulsed for Ramsey spectroscopy by switching on and off the rf signal sent to the AOM to create the *CPT* pulses. The first *CPT* pulse pumps the atoms into the dark state, and its duration is typically between 0.4 and 1 ms. After a Ramsey period of typically  $T_R = 16$  ms, the atoms are probed by a second 0.05-ms *CPT* pulse.

Per experimental cycle, four signals are measured that are used to construct the *CPT* resonances—the power transmitted through the atoms and measured on the *CPT* photodiode during the first and second pulses,  $T_1$  and  $T_2$ , and the signals from the normalization photodiode during each signal detection,  $N_1$  and  $N_2$ . Two types of *CPT* spectra can be calculated from these signal voltages when the modulation frequency to the EOM is scanned—single-pulse spectra and double-pulse “Ramsey”-type spectra. To measure single-pulse spectra, the average photodiode signals are measured for the final 300  $\mu\text{s}$  of the first *CPT* pulse and the normalized signal  $S_{1-\text{pulse}} = T_1/N_1$  is plotted versus Raman detuning. Ramsey spectra are constructed from the average photodiode signals for the first 50  $\mu\text{s}$  of the second pulse. The Ramsey spectra are typically normalized by dividing the transmission at the beginning of the second pulse by the transmission at the end of the first pulse, such that the plotted value is  $S_{\text{Ramsey}} = (T_2/N_2)/(T_1/N_1)$ , which usually makes the Ramsey spectra more symmetric and normalizes them against atom number fluctuations.

When the experiment is run as a clock, the sides of the central Ramsey fringe are alternately probed by modulating

the microwave frequency that drives the EOM. The microwave reference frequency is alternated between values of  $\nu_0 - \Delta\nu/2$  and  $\nu_0 + \Delta\nu/2$  from cycle to cycle, where  $\Delta\nu = 1/2T_R$  is the width of the central Ramsey fringe and  $\nu_0$  is the estimate of the hyperfine ground-state splitting on which the central fringe is centered. The Ramsey signal  $S_{\text{Ramsey}}$  is measured for these two frequency set points, and the value of  $\nu_0$  is steered based on the best estimate of the frequency of the central Ramsey fringe to lock the average microwave frequency to the central fringe. The frequency stability is characterized by a calculation of the Allan deviation of the frequency steers that are executed that keep the synthesizer locked to the atomic resonance.

### III. MEASUREMENTS

#### A. Single-pulse and Ramsey spectra

*CPT* signals based on the absorption during the first *CPT* pulse in the lin || lin *CPT* scheme for the low-coherence OPLL and the high-coherence EOM interrogation systems are shown in Fig. 3. The improved coherence of the *CPT* light generated with the EOM directly increases the absorption contrast of the *CPT* resonance signal, where the absorption contrast characterizes the completeness of dark-state formation. The absorption contrast is defined as the ratio of the *CPT* peak height ( $A$ ) to the height of the optical absorption signal ( $B$ ) [see Fig. 3(a)]. The absorption contrast of the *CPT* resonance in the EOM-based setup is increased by more than a factor of 2 compared to the OPLL system. For EOM interrogation, the resonant absorption goes nearly to zero with a contrast of  $> 95\%$ , which indicates the formation of a nearly complete dark state. This high absorption contrast is possible because there are no significant sources of decoherence in the cold-atom system.

A Ramsey spectrum measured in the lin || lin *CPT* scheme is shown in Fig. 4, with the inset showing the central fringes on a narrower frequency scale.

#### B. Light shifts

In previous theories for the light shift of *CPT* clocks based on Ramsey spectroscopy [18,19], the resonant light shift vanishes when the intensity and the duration of the pumping pulse are sufficient and the atoms can reach a completely dark equilibrium state during the first *CPT* interrogation pulse. To a very good approximation, when the optical detuning  $\delta$  is much smaller than the optical linewidth  $\gamma$ , the phase shift  $\phi$  of the central Ramsey fringe can be expressed as [18,19]

$$\tan \phi = -d\rho \sin(\Omega^2 \delta \tau_1 / \gamma^2) \exp(-\Omega^2 \tau_1 / \gamma). \quad (1)$$

Here,  $\Omega^2$  is the average squared Rabi frequency of the two frequency components of the *CPT* light and  $\tau_1$  is the duration of the first *CPT* pulse.  $d\rho$  is the initial population difference between the two hyperfine ground states at the start of a Ramsey cycle.

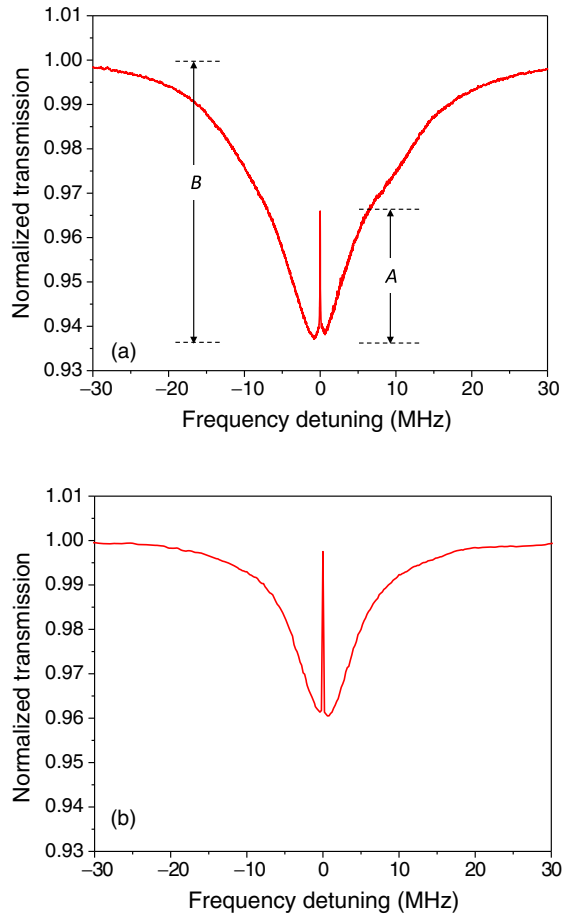


FIG. 3. Single-pulse *CPT* transmission signals detected with the (a) OPLL- and (b) EOM-based light sources collected with no averaging—each point in the spectra results from a single measurement on a single sample of MOT atoms. The absorption contrast  $A/B > 95\%$  for the EOM system. To perform these measurements, the carrier frequency is held fixed and locked to the  $F = 2 \rightarrow F' = 1$  optical transition while the modulation frequency to the EOM is scanned. The optical resonances are slightly offset from the *CPT* resonances because of small offsets of the laser lock for the carrier frequency in the saturated absorption spectrometer. The optical intensities are  $0.072$  and  $0.18$   $\text{mW}/\text{cm}^2$ , respectively. The main reason for the higher optical absorption ( $B$ ) on resonance in the earlier OPLL configuration is that there are only two frequency components in the OPLL spectrum. The EOM spectrum contains a strong unwanted sideband that is roughly equal in intensity to the carrier and first-order sidebands that are used for *CPT* interrogation. Small bumps in the spectrum in (b) result from residual intensity fluctuations in the system.

It was previously shown that imperfect phase coherence between the *CPT* fields can lead to light shifts that do not vanish at high intensities, as predicted by Eq. (1), and that have a strong dependence on optical detuning [21]. Figure 5 shows the magnitude of the fractional frequency shift versus the optical intensity of the *CPT* light per megahertz of optical detuning for the low- and high-coherence systems. Compared to the OPLL-based system, the magnitude of the frequency shift versus the optical

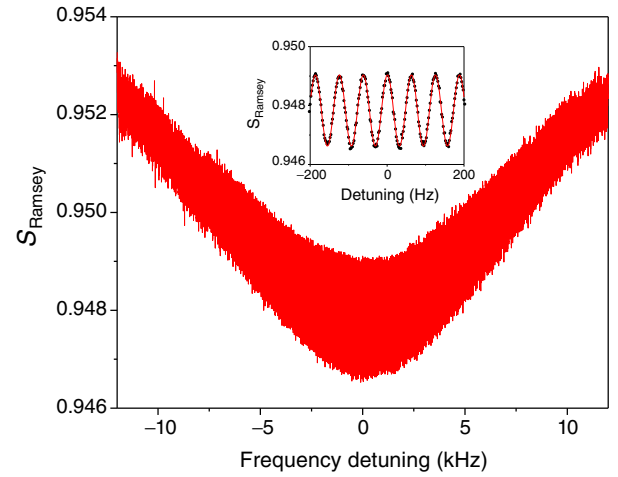


FIG. 4. A typical Ramsey spectrum measured with the high-coherence light source based on an EOM. The optical intensity is  $0.27$   $\text{mW}/\text{cm}^2$ . (Inset) Enlargement of the central Ramsey fringes fitted to a sine function showing a SNR ratio of 38 in a cycle period of  $T_c = 43.49$  ms (no averaging). This SNR corresponds to a SNR of 180 in a 1-Hz bandwidth.

detuning at high intensity is reduced by approximately 2 orders of magnitude.

Similar decaying behavior is seen when, instead of varying the intensity, the length of the first Ramsey pulse is varied. This decay versus pump time is shown in Fig. 6,

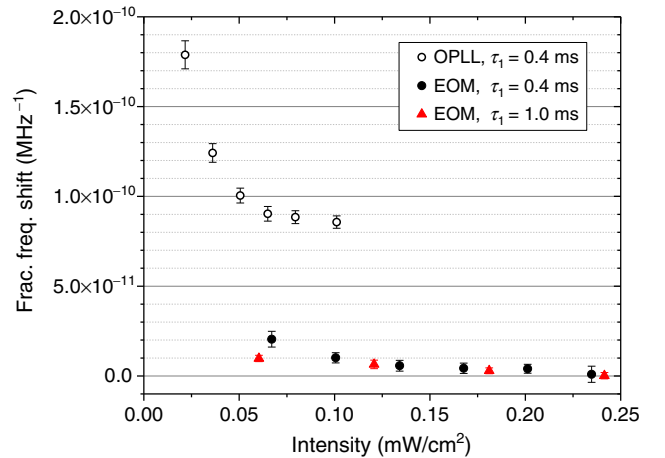


FIG. 5. Comparison of the resonant light shift per megahertz of optical detuning versus intensity for the OPLL- and EOM-based systems. The duration of the Ramsey period is 16 ms. Here, the intensity is the total intensity (forward and backward beams) and the intensities of the two *CPT* components are equal. The intensity scale of the EOM-based data has been multiplied by a factor of  $2/3$  to account for the presence of the unwanted sideband that contains about  $1/3$  of the optical power. These measurements are performed with the lin || lin interrogation scheme. The EOM data for two different pump-pulse lengths are very similar because the atoms nearly reach a dark-state equilibrium even for the shorter pump-pulse duration.

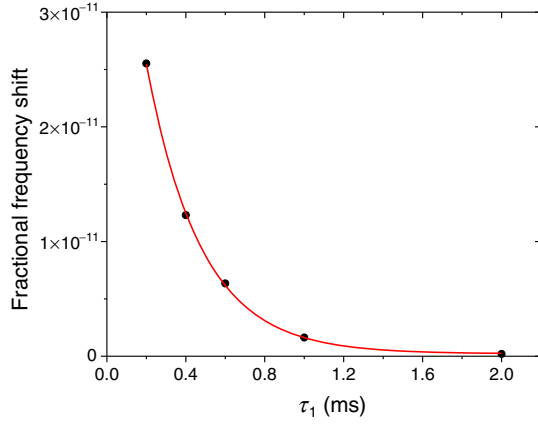


FIG. 6. Fractional frequency shift for 2-MHz optical detuning versus the length of the first pulse,  $\tau_1$ . The total input intensity is fixed at  $I_{\text{CPT}} = 0.15 \text{ mW/cm}^2$ , and the Ramsey period is  $T_R = 16 \text{ ms}$ . The black dots represent the experimental data. The red solid line is a fit of a simple decaying exponential function, which gives a value of  $0.28(1) \text{ ms}$  for the decay time constant under these conditions. This decay time constant motivates the usual choice of  $\tau_1 = 1 \text{ ms}$ . Note that these data cannot be fit to Eq. (1) without large errors because of the nonlinear nature of the shift. In past studies where the shift was deliberately made much larger [21], the theoretical model [18,19] could be well fit to observed shifts with no adjustable parameters.

which plots the average magnitude of the fractional frequency shift of the central Ramsey fringe for an optical detuning of 2 MHz as a function of  $\tau_1$  with the high-coherence EOM-based system.

### C. Frequency stability

With the highly coherent EOM-based light source, the short-term frequency stability of the clock is typically  $1.6 \times 10^{-11}/\sqrt{\tau}$  and consistently achieves  $3 \times 10^{-13}$  at a 1-h integration period (Fig. 7). For comparison, a typical Allan deviation for the low-coherence OPLL-based system is also

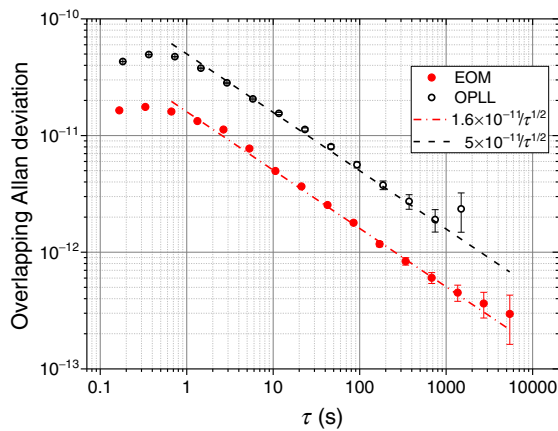


FIG. 7. Frequency stability of the cold-atom *CPT* clock based on lin || lin interrogation comparing interrogation with an OPLL-based system and an EOM-based system.

shown in Fig. 7. The short-term stability is about 3 times better with the high-coherence system than with the low-coherence OPLL. The long-term stabilities are typically about an order of magnitude better with the high-coherence system, which is attributed to the reduction of the resonant light shift resulting from nearly complete dark-state formation.

*CPT* clocks based on thermal vapor cells have demonstrated significantly better short-term stability than the cold-atom clock presented here, by as much as a factor of 50 (See Ref. [9]). This higher stability is partially because vapor-cell clocks interrogate about  $1000\times$  more atoms than are interrogated in the cold-atom clock presented here, which affects the SNR. However, the short-term stability presented in Fig. 7 is about  $50\times$  worse than the stability limited by atom shot noise, which indicates that the stability can be improved if the noise contributions can be reduced. The real advantage of cold-atom clocks over clocks based on thermal vapor cells is in improved long-term stability. The long-term stability for the clock presented here is about 3 times better than for the vapor-cell *CPT* clocks that show the best short-term stability [9] on time scales of an hour.

Rough estimates of the noise contributions to the SNR of the *CPT* signals from various sources have been investigated by measuring the *CPT* transmission fluctuations under various conditions, including with and without atoms present and on the top and the side of the central Ramsey fringe. Integrated shot-to-shot photodiode signal variations have been used to determine the contribution to the noise on the *CPT* Ramsey spectra from electronic noise, laser intensity noise, laser frequency noise, and microwave phase fluctuations. The three dominant noise sources with roughly equal contributions are laser intensity noise, laser frequency noise, and microwave phase fluctuations.

## IV. DISCUSSION AND SUMMARY

The resonant light shift was a dominant factor limiting the long-term frequency stability of a cold-atom *CPT* clock that employed a low-coherence OPLL-based light source [21], which was a result of incomplete dark-state formation. OPLL systems can generally provide a high degree of phase control when the loop bandwidths are significantly larger than the laser linewidths [40]. This condition was not met by the OPLL implementation in Ref. [20], where the FM bandwidth was limited by the slowness of the laser diode's frequency response. While single-section diode lasers are convenient for their simplicity and compactness, a disadvantage they present to phase locking is that they typically exhibit a phase reversal in their frequency-modulation response in the (0.5–10)-MHz range due to the crossover between thermally and carrier-density-induced tuning regimes. This effect limits the maximum bandwidth of the OPLL in the system to less than 1 MHz, which results in an interrogation spectrum where only about 70% of the total power is coherent. The rest of the

power is in a broad noise pedestal on the slave laser that spans a frequency range of about 20 MHz.

Because the incoherent light in the OPLL-generated spectrum causes relaxation of the dark-state coherence, the light shift does not vanish at high optical intensity. Switching to a high-coherence laser system based on an EOM dramatically reduces the resonant light shift such that it is no longer a dominant limiting factor for the clock's long-term frequency stability.

The long-term stability achieved in the high-coherence interrogation system is comparable to the stability of published results for two other recently developed compact microwave clocks based on laser-cooled atoms and direct microwave interrogation [41,42]. It is also competitive with a recently developed ion clock based on warm  $^{171}\text{Yb}$  atoms [43].

There are many examples of high-performance *CPT* clocks based on vapor cells in the literature [16,17,44–46]. Some of these have achieved short-term frequency instabilities on the low  $10^{-13}$  scale [9,30,47], or they have been averaged down to that level after a few-hundred seconds [16,17,45]. A common feature of all of these *CPT* clocks is that drift becomes significant on time scales from a few-hundred to a few-thousand seconds as the instability increases for longer integration periods [9,10,16,17,30,44,46,47].

Thus far, most of the cold-atom *CPT* studies performed with the system described here have been done with the lin || lin polarization scheme, but cold-atom clocks can benefit from other polarization schemes in the form of simplified spectra and reduced Zeeman shifts (for a review, see Ref. [48]). Light shifts from off-resonant hyperfine transitions are currently under investigation. Off-resonant shifts were studied previously for *CPT* clocks using continuous excitation [17], where it was shown that the light shift could be reduced through adjustment of the optical spectrum via changes in the modulation index. With Ramsey spectroscopy, the size of the shifts follows the same dependence on modulation index, but the overall size of the shifts can be made much smaller and can also be better controlled with other polarization schemes. Future *CPT* clocks may also demonstrate smaller shifts from the use of autobalanced Ramsey techniques [49] adapted for coherent population trapping.

## ACKNOWLEDGMENTS

J. Elgin, A. Hansen, M. Lombardi, C. Oates, and J. W. Pollock are gratefully acknowledged for the technical help and discussions. V.I.Y. was supported by the Russian Science Foundation (Grant No. 16-12-10147), the Ministry of Education and Science of the Russian Federation (Grant No. 3.1326.2017/4.6), and the Russian Foundation for Basic Research (Grant No. 17-02-00570). This article is a contribution of the U.S. Government, not subject to U.S. copyright.

- [1] L. S. Cutler, Fifty years of commercial caesium clocks, *Metrologia* **42**, S90 (2005).
- [2] R. F. C. Vessot, The atomic hydrogen maser oscillator, *Metrologia* **42**, S80 (2005).
- [3] W. J. Riley, *Rubidium Frequency Standard Primer* (Hamilton Technical Services, Beaufort, SC, 2011).
- [4] G. Alzetta, A. Gozzini, L. Moi, and G. Orriols, An experimental method for the observation of r.f. transitions and laser beat resonances in oriented Na vapour, *Nuovo Cimento Soc. Ital. Fis.* **36B**, 5 (1976).
- [5] E. Arimondo, Coherent population trapping in laser spectroscopy, *Prog. Opt.* **35**, 257 (1996).
- [6] J. Vanier, Atomic clocks based on coherent population trapping: A review, *Appl. Phys. B* **81**, 421 (2005).
- [7] S. Knappe, V. Shah, P. D. D. Schwindt, L. Hollberg, J. Kitching, L.-A. Liew, and J. Moreland, A microfabricated atomic clock, *Appl. Phys. Lett.* **85**, 1460 (2004).
- [8] R. Lutwak, P. Vlitras, M. Varghese, M. Mescher, D. K. Serkland, and G. M. Peake, in *Proceedings of the IEEE International Frequency Control Symposium and Exposition, Vancouver, 2005* (IEEE, New York, 2005), p. 752.
- [9] P. Yun, F. Tricot, C. E. Calosso, S. Micalizio, B. François, R. Boudot, S. Gurandel, and E. de Clercq, High-Performance Coherent Population Trapping Clock with Polarization Modulation, *Phys. Rev. Applied* **7**, 014018 (2017).
- [10] M. A. Hafiz, G. Coget, P. Yun, S. Gurandel, E. de Clercq, and R. Boudot, A high-performance Raman-Ramsey Cs vapor cell atomic clock, *J. Appl. Phys.* **121**, 104903 (2017).
- [11] R. Lutwak, A. Rashed, M. Varghese, G. Tepolt, J. Leblanc, M. Mescher, D. K. Serkland, and G. M. Peake, in *Proceedings of the IEEE International Frequency Control Symposium Joint with the 21st European Frequency and Time Forum, Geneva, Switzerland, 2007* (IEEE, New York, 2007), p. 1327.
- [12] R. Lutwak, A. Rashed, M. Varghese, G. Tepolt, J. LeBlanc, M. Mescher, D. K. Serkland, K. M. Geib, G. M. Peake, and S. Romisch, in *Proceedings of the 39th Annual Precise Time and Time Interval Meeting, Long Beach, California, 2007* (The Institute of Navigation, Manassas, VA, 2007), p. 269.
- [13] J. Vanier and C. Audoin, *The Quantum Physics of Atomic Frequency Standards* (Adam Hilger, Bristol, England, 1992).
- [14] J. Vanier, M. W. Levine, S. Kendig, D. Janssen, C. Everson, and M. J. Delaney, Practical realization of a passive coherent population trapping frequency standard, *IEEE Trans. Instrum. Meas.* **54**, 2531 (2005).
- [15] R. Boudot, S. Guerandel, E. de Clercq, N. Dimarcq, and A. Clairon, Current status of a pulsed *CPT* Cs cell clock, *IEEE Trans. Instrum. Meas.* **58**, 1217 (2009).
- [16] N. Castagna, R. Boudot, S. Gurandel, E. D. Clercq, N. Dimarcq, and A. Clairon, Investigations on continuous and pulsed interrogation for a *CPT* atomic clock, *IEEE Trans. Ultrason. Ferroelectr. Freq. Control* **56**, 246 (2009).
- [17] M. Zhu and L. S. Cutler, in *Proceedings of the 32nd Annual Precise Time and Time Interval Systems and Applications Meeting, Reston, VA, 2000* (The Institute of Navigation, Manassas, VA, 2000), p. 311.
- [18] P. R. Hemmer, M. S. Shahriar, V. D. Natoli, and S. Ezekiel, ac Stark shifts in a two-zone Raman interaction, *J. Opt. Soc. Am. B* **6**, 1519 (1989).
- [19] M. S. Shahriar, P. R. Hemmer, D. P. Katz, A. Lee, and M. G. Prentiss, Dark-state-based three-element vector model for

- the stimulated Raman interaction, *Phys. Rev. A* **55**, 2272 (1997).
- [20] F.-X. Esnault, E. Blanshan, E. N. Ivanov, R. E. Scholten, J. Kitching, and E. A. Donley, Cold-atom double- $\Lambda$  coherent population trapping clock, *Phys. Rev. A* **88**, 042120 (2013).
- [21] E. Blanshan, S. M. Rochester, E. A. Donley, and J. Kitching, Light shifts in a pulsed cold-atom coherent-population-trapping clock, *Phys. Rev. A* **91**, 041401 (2015).
- [22] N. F. Ramsey, A molecular beam resonance method with separated oscillating fields, *Phys. Rev.* **78**, 695 (1950).
- [23] J. E. Thomas, P. R. Hemmer, S. Ezekiel, C. C. Leiby, R. H. Picard, and C. R. Willis, Observation of Ramsey Fringes Using a Stimulated, Resonance Raman Transition in a Sodium Atomic Beam, *Phys. Rev. Lett.* **48**, 867 (1982).
- [24] P. R. Hemmer, S. Ezekiel, and J. C. C. Leiby, Stabilization of a microwave oscillator using a resonance Raman transition in a sodium beam, *Opt. Lett.* **8**, 440 (1983).
- [25] P. R. Hemmer, G. P. Ontai, and S. Ezekiel, Precision studies of stimulated-resonance raman interactions in an atomic beam, *J. Opt. Soc. Am. B* **3**, 219 (1986).
- [26] P. R. Hemmer and M. G. Prentiss, Coupled-pendulum model of the stimulated resonance raman effect, *J. Opt. Soc. Am. B* **5**, 1613 (1988).
- [27] T. Zanon, S. Guerandel, E. de Clercq, D. Holleville, N. Dimarcq, and A. Clairon, in *Proceedings of the 18th European Frequency and Time Forum, Guildford, England, 2004* (The Institution of Engineering and Technology, London, 2004), p. 29.
- [28] J.-M. Danet, M. Lours, P. Yun, S. Guerandel, and E. de Clercq, in *Proceedings of the 2013 Joint European Frequency and Time Forum and International Frequency Control Symposium, Prague, 2013* (IEEE, New York, 2013), p. 586.
- [29] X. Liu, J. M. Mrolla, S. Guerandel, E. de Clercq, and R. Boudot, Ramsey spectroscopy of high-contrast *CPT* resonances with push-pull optical pumping in Cs vapor, *Opt. Express* **21**, 12451 (2013).
- [30] J.-M. Danet, O. Kozlova, P. Yun, S. Guerandel, and E. de Clercq, Compact atomic clock prototype based on coherent population trapping, *EPJ Web Conf.* **77**, 00017 (2014).
- [31] O. Kozlova, J.-M. Danet, S. Guerandel, and E. de Clercq, Limitations of long-term stability in a coherent population trapping Cs clock, *IEEE Trans. Instrum. Meas.* **63**, 1863 (2014).
- [32] Y. Yano, W. Gao, S. Goka and M. Kajita, Theoretical and experimental investigation of the light shift in Ramsey coherent population trapping, *Phys. Rev. A* **90**, 013826 (2014).
- [33] A. V. Taichenachev, V. I. Yudin, V. L. Velichansky, and S. A. Zibrov, On the unique possibility of significantly increasing the contrast of dark resonances on the *D1* line of  $^{87}\text{Rb}$ , *JETP Lett.* **82**, 398 (2005).
- [34] E. Breschi, G. Kazakov, R. Lammegger, G. Miletì, B. Matisov, and L. Windholz, Quantitative study of the destructive quantum-interference effect on coherent population trapping, *Phys. Rev. A* **79**, 063837 (2009).
- [35] S. A. Zibrov, I. Novikova, D. F. Phillips, R. L. Walsworth, A. S. Zibrov, V. L. Velichansky, A. V. Taichenachev, and V. I. Yudin, Coherent-population-trapping resonances with linearly polarized light for all-optical miniature atomic clocks, *Phys. Rev. A* **81**, 013833 (2010).
- [36] E. E. Mikhailov, T. Horrom, N. Belcher, and I. Novikova, Performance of a prototype atomic clock based on lin || lin coherent population trapping resonances in Rb atomic vapor, *J. Opt. Soc. Am. B* **27**, 417 (2010).
- [37] H. J. McGuinness, A. V. Rakholia, and G. W. Biedermann, High data-rate atom interferometer for measuring acceleration, *Appl. Phys. Lett.* **100**, 011106 (2012).
- [38] A. V. Taichenachev, V. I. Yudin, V. L. Velichansky, S. V. Kargapoltsev, R. Wynands, J. Kitching, and L. Hollberg, High-contrast dark resonances on the *D1* line of alkali metals in the field of counterpropagating waves, *JETP Lett.* **80**, 236 (2004).
- [39] S. V. Kargapoltsev, J. Kitching, L. Hollberg, A. V. Taichenachev, V. L. Velichansky, and V. I. Yudin, High-contrast dark resonance in  $\sigma_+ - \sigma_-$  optical field, *Laser Phys. Lett.* **1**, 495 (2004).
- [40] J. Ye and J. L. Hall, Optical phase locking in the microradian domain: Potential applications to NASA spaceborne optical measurements, *Opt. Lett.* **24**, 1838 (1999).
- [41] V. Shah, M. Mescher, A. Martins, J. Leblanc, N. Byrne, B. Timmons, R. Stoner, F. Rogamentich, and R. Lutwak, in *Proceedings of the 43rd Annual Precise Time and Time Interval (PTTI) Systems and Applications Meeting, Long Beach, CA, 2011* (The Institute of Navigation, Manassas, VA, 2011), p. 221.
- [42] J. Sebby-Strabley, K. Salit, K. Nelson, J. Ridley, and J. Kriz, in *Proceedings of the 43rd Annual Precise Time and Time Interval (PTTI) Systems and Applications Meeting, Long Beach, CA, 2011* (The Institute of Navigation, Manassas, VA, 2011), p. 231.
- [43] Y. Y. Jau, H. Partner, P. D. D. Schwindt, J. D. Prestage, J. R. Kelllogg, and N. Yu, Low-power, miniature  $^{171}\text{Yb}$  ion clock using an ultra-small vacuum package, *Appl. Phys. Lett.* **101**, 253518 (2012).
- [44] S. Knappe, R. Wynands, J. Kitching, H. G. Robinson, and L. Hollberg, Characterization of coherent population-trapping resonances as atomic frequency references, *J. Opt. Soc. Am. B* **18**, 1545 (2001).
- [45] M. Zhu, in *Proceedings of the IEEE International Frequency Control Symposium and PDA Exhibition Jointly with the 17th European Frequency and Time Forum, Tampa, 2003* (IEEE, New York, 2003), p. 16.
- [46] M. Merimaa, T. Lindvall, I. Tittonen, and E. Ikonen, All-optical atomic clock based on coherent population trapping in  $^{85}\text{Rb}$ , *J. Opt. Soc. Am. B* **20**, 273 (2003).
- [47] M. A. Hafiz and R. Boudot, A coherent population trapping Cs vapor cell atomic clock based on push-pull optical pumping, *J. Appl. Phys.* **118**, 124903 (2015).
- [48] Z. Warren, M. S. Shahriar, R. Tripathi, and G. S. Pati, Experimental and theoretical comparison of different optical excitation schemes for a compact coherent population trapping Rb vapor clock, *Metrologia* **54**, 418 (2017).
- [49] C. Sanner, N. Huntemann, R. Lange, C. Tamm, and E. Peik, Auto-balanced Ramsey spectroscopy, [arXiv: 1707.02630](https://arxiv.org/abs/1707.02630).